Molecular mechanism regulating transcriptional control of the *hig* toxin-antitoxin locus of antibiotic-resistance plasmid Rts1 from *Proteus vulgaris*

Ian Pavelich[1,2], Marc A. Schureck[1], Dongxue Wang[1], Eric D. Hoffer[1], Michelle Boamah[1], Nina Onuoha[1], Stacey J. Miles[1], C. Denise Okafor[3], and Christine M. Dunham[1]*

[1]Department of Biochemistry and the Emory Antibiotic Resistance Center, Emory University School of Medicine, Atlanta, Georgia, 30322

[2]Department of Chemistry, Emory University, Atlanta, Georgia, 30322

[3]Department of Biochemistry and Molecular Biology, Pennsylvania State University, University Park, Pennsylvania 16802

These authors contributed equally.

*To whom correspondence should be addressed: Tel: 1-404-712-1756; Fax: 1-404-727-2738; Email: christine.m.dunham@emory.edu

Data deposition: Crystallography, atomic coordinates, and structure factors have been deposited in the Protein Data Bank, www.pdb.org (PDB codes 6W6U, 6WFP)

Running title: Regulation of *P. vulgaris* HigBHigA toxin-antitoxin

Keywords: toxin-antitoxin complexes, gene expression regulation, transcriptional repression, DNA-binding proteins, X-ray crystallography, *Proteus vulgaris*

ABSTRACT

Regulation of ubiquitous bacterial type II toxin-antitoxin (TA) gene pairs occurs via a negative feedback loop whereby their expression is typically responsive to changing levels of toxins at the transcriptional level similar to a molecular rheostat. While this mechanism can explain how certain TA complexes are regulated, accumulating evidence suggests diversity in this regulation. One system for which the negative feedback loop is not well defined is the plasmid-encoded HigBHigA TA pair originally identified in a post-operative infection with antibiotic resistant *Proteus vulgaris*. In contrast to other type II TA modules, each *hig* operator functions independently and excess toxin does not contribute to increased transcription *in vivo*. Structures of two different oligomeric complexes of HigBHigA bound to its operator DNA reveal similar interactions are maintained suggesting plasticity in how *hig* is repressed. Consistent with this result, molecular dynamic simulations reveal both oligomeric states exhibit similar dynamics. Further, engineering a dedicated trimeric HigBHigA complex does not regulate transcriptional repression. We propose that HigBHigA functions via a simple on/off transcriptional switch regulated by antitoxin proteolysis rather than a molecular rheostat. The present studies thus expand the known diversity of how these abundant bacterial protein pairs are regulated.

IMPORTANCE

Bacteria respond to various stimuli by rapidly regulating gene expression to control growth. The diversity in how bacteria inhibit growth is exemplified by the abundance and diversity of toxin-antitoxin (TA) gene pairs. To tightly regulate their own expression, antitoxin proteins function as transcriptional autorepressors with additional regulation imparted by responsiveness of the system to toxin concentrations, similar to a molecular rheostat. However, some TAs do not appear to be responsive to changing levels of toxin. To expand our understanding of diverse TAs, we studied the regulation of a structurally distinct TA called host inhibition of growth (HigBA) originally discovered on the antibiotic resistance Rts1 plasmid associated with *Proteus vulgaris*. We find that the *hig* operon is regulated via a simple on/off transcriptional switch that is incalcitrant to changing toxin levels. These results expand the known mechanistic diversity of how TA pairs regulate their expression.

INTRODUCTION

Bacterial toxin-antitoxin (TA) genes are bicistronic operons found in mobile genetic elements and bacterial chromosomes (1-3). Type II TA modules consist of toxin and antitoxin protein components that form architecturally diverse macromolecular complexes in the absence of external stimuli and during nutrient-rich growth. Although these gene pairs were first identified on plasmids and in bacteriophages (4-9), TAs are highly abundant in free-living bacteria where they appear to have different functions. In their role in plasmid maintenance, the toxin component can induce post-segregational killing if both genes are not inherited (6). In the past few years, conflicting experimental data on the endogenous activities of TAs have led to ambiguity and controversy surrounding their roles in bacterial physiology (10).

Regulation of type II TA pairs frequently occurs at the transcriptional level via a negative feedback loop (10-12). Antitoxin proteins contain a DNA-binding motif and repress at operator sites that overlap with promoters of TA genes. Toxin proteins are either recruited to their cognate antitoxins bound at these operator sites or bind to operators as TA complexes where they function as co-repressors, allowing the system to be responsive to changes in toxin expression levels. Further, TAs can form different oligomeric complexes when bound at operator sites that alter their binding thermodynamics to result in a gradient of the transcriptional response similar to a molecular rheostat (13, 14). This response gradient can also be influenced by cooperative TA binding at adjacent operator sites; this process is known as “conditional cooperativity” (15-18). However, this model is dependent on the architectural organization of TAs pairs which can diverge significantly (12, 19). Thus, it is unclear if conditional cooperativity can explain the regulation of all type II TA systems.

The structural diversity and distinct toxin- and DNA-binding motifs of different type II antitoxin proteins may partially explain why they can exert different mechanisms of autoregulation (11). Antitoxins contain ribbon-helix-helix (RHH), helix-turn-helix (HTH),

Phd/YefM or SpoVT/AbrB DNA-binding motifs, with RHH and HTH being the most common (20-26). The type of DNA binding motif affects transcriptional repression. HTH-containing antitoxins contain a complete DNA-binding motif while RHH-containing antitoxins contain a half site requiring antitoxin dimerization for DNA binding. TA operons usually contain multiple operator sites and antitoxin binding at adjacent sites can lead to cooperativity and an increase in transcriptional repression (17, 18, 27). Antitoxins are particularly susceptible to proteases especially during changing cellular conditions (28). This reduction in antitoxin concentration increases free toxin levels that when free, can inhibit growth. Free toxin can also interact with antitoxins bound at their operators changing the oligomeric state of the TA complex during repression. These oligomeric state changes, in turn, can lead to differences in the ability of TAs to bind their operator and influence the extent of repression; effectively this responsiveness allows the system to function as a molecular rheostat (**Fig. 1**). In contrast, other TA systems do not appear to be responsive to changing levels of toxin and instead are simple on/off transcriptional switches (29, 30). While there exists some experimental evidence that distinguishes between the molecular rheostat and the on/off switch modes of regulation, at present the molecular basis for each mechanism is ambiguous because there is little or no structural evidence as a foundation for each model.

The *host inhibition of growth* BA (*higBA*) TA module seems to function as an on/off switch. The HigBHigA pair was first identified on the antibiotic-resistance plasmid Rts1 associated with *Proteus vulgaris* and discovered post-operatively in an urinary tract infection (31, 32) (we call this TA pair “HigBHigA” to denote both the HigB toxin and HigA antitoxin proteins). The HigB toxin belongs to the RelE family of toxins, resembles a microbial ribonuclease and cleaves mRNA substrates bound to a translating ribosome (26, 33-35). Although there are HigBHigA TA pairs found chromosomally and these HigB toxins are also RelE family members (36, 37), the structural organization and the regulation of these

systems compared to the *P. vulgaris* associated module seems to be different (26). While all known HigA homologs contain a HTH DNA-binding motif, the *P. vulgaris* associated antitoxin binds to each of its operator sites (O1 and O2) in a non-cooperative manner (26, 38). Here, we test the two models of transcriptional regulation, rheostat versus on/off switch, to determine the molecular mechanism of action of HigBHigA.

RESULTS

Transcriptional repression at each operator is independently regulated. The *hig* promoter (P*hig*) is negatively autoregulated by the HigBHigA complex binding at operators O1 and O2 that overlap with the -35 and -10 promoter sites (32) (**Fig. 2A**). The HigBHigA complex forms a tetrameric assembly with two HigB monomers and a HigA dimer ($HigB_2HigA_2$) (26). Each HigA antitoxin contains a single HTH DNA-binding motif and forms an obligate dimer, meaning that two HigA antitoxins in one $HigB_2HigA_2$ complex bind two inverted repeats of a single DNA operator (26, 38). To determine if we could build oligomeric complexes *in vitro*, we monitored the binding of the $HigB_2HigA_2$ complex to *hig* (O1 and O2) using an electrophoretic mobility shift assay (EMSA) (**Fig. 2B**). The $HigB_2HigA_2$ complex was purified according to previously published protocols and the DNA probe used in the EMSA consists of the entire 61 basepair (bp) operator region (**Table S1**). Titration of $HigB_2HigA_2$ with a constant amount of *hig* causes two molecular weight shifts, indicating binding of $HigB_2HigA_2$ at each operator site (**Fig. 2B**, top). To determine whether $HigB_2HigA_2$ binds with a higher affinity to either O1 or O2, all 21 nucleotides in each operator were randomized individually (38). Each of these 21 nucleotides located in either O1 or O2 were previously shown to be protected upon HigA binding (39). Therefore any change in the mobility of the DNA band using a scrambled O1 or O2 would represent binding of $HigB_2HigA_2$ to a single operator. $HigB_2HigA_2$ binds to each of the two sites represented as a single

molecular weight shift and both result in similar dissociation binding constants (0.36 ± 0.09 μM for O1 and 0.24 ± 0.04 μM for O2) (**Fig. 2B**, middle and lower; **Table S2**). These data indicate that $HigB_2HigA_2$ recognizes each operator independently to form a high affinity interaction. This observation appears to be an important distinction from other type II TAs where TA complexes binding at an operator influences the binding of TAs at adjacent operators (**Fig. 1**).

To test whether $HigB_2HigA_2$ binding at a single operator results in transcriptional repression *in vivo*, we designed a series of constructs that encode *lacZ* in three different contexts: downstream of the P*hig* promoter (pQF50-P*hig*-*lacZ*), downstream of wild-type HigA (pQF50-P*hig*-*higA*-*lacZ*), or downstream of a C-terminally truncated HigA (pQF50-P*hig*-*higA*(Δ84-104)-*lacZ*) (**Fig. 2C**). The pQF50-P*hig*-*lacZ* construct reports on the activity of P*hig* in the absence of repressor HigA, while the HigA-encoding pQF50-P*hig*-*higA*-*lacZ* construct reports on how expression of HigA represses P*hig*. The third construct serves as a control as the HigA(Δ84-104) variant is unable to dimerize and bind P*hig* but is comparably expressed (26, 38). P*hig*-*lacZ* shows robust β-galactosidase (β-gal) activity which we normalize to represent complete transcriptional repression (this is represented as 0% repression; **Fig. 2C**). Expression of HigA efficiently represses P*hig*, whereas HigA(Δ84-104) restores P*hig* activity to near P*hig*-only levels, indicating transcriptional repression is dependent on HigA expression and dimerization (**Fig. 2C**). To test whether $HigA_2$ binding to a single operator region is sufficient for repression, we mutated either O1 or O2 recognition sequences important for HigA binding (38) and repeated the previously described β-gal assays. Mutations to either O1 ($G_{-24}T/C_{-30}A$) or O2 ($G_{-8}T/C_{-2}A$) do not affect $HigA_2$ repression at a single mutant P*hig* when compared to the wild-type P*hig* (**Fig. 2C**, compare middle bars in “O1 variant” and “O2 variant” group to “P*hig*”). These results show that $HigA_2$ binding at either O1 or O2 is sufficient for repression (data also presented in Miller Units in **Fig. S1**).

Further, these data indicate that $HigA_2$ binding at each *hig* operator is not cooperative, and that a single operator is sufficient for transcriptional repression.

Addition of HigB destabilizes interactions between HigA and DNA *in vitro*. The expression of most type II TA complexes is regulated at the transcriptional level by changing toxin and antitoxin concentrations as a result of increased proteolysis of the antitoxin during external stimuli (17, 18, 22). We reasoned that the HigBHigA complex may transcriptionally repress using a different mechanism because of the structural diversity of the HigA antitoxin. The unique structure of HigA could influence its interactions with *hig* or HigB toxin binding. For example, the HigA HTH motif is a complete DNA-binding domain and by extension, the obligate $HigA_2$ dimer contains two DNA-binding domains. Other type II antitoxins typically contain a single DNA-binding motif formed by antitoxin dimerization (**Fig. 1**). These differences are likely important for the changing of different oligomeric TA complexes bound to operators allowing the system to respond to changing toxin levels. To test this, we explored whether the presence of excess HigB changes the molecular interactions of HigA with the O1-O2 operators (**Fig. 3**). Addition of $HigA_2$ to O1-O2 results in two shifted bands of lower mobility, indicative of complexes with a single $HigA_2$ dimer bound to one operator (**Fig. 3A**, **yellow**), or two $HigA_2$ dimers binding to each operator (**Fig. 3A, orange**). Increasing amounts of HigB results in the formation of two additional higher molecular weight species (**Fig. 3A**). In this case, either the HigB monomer binds to each of the $HigA_2$ dimers to form a trimeric $HigBHigA_2$ complex (**Fig. 3A, red**) or both HigB monomers bind to a single $HigA_2$ dimer as a tetrameric $HigB_2HigA_2$ (**Fig. 3A, purple**). As the $HigA_2$ dimer is already bound at both O1 and O2, it is unlikely that the molecular weight species would represent occupation of only a single operator site. While the third shift may contain a mixed population of oligomeric states where HigB binds only one $HigA_2$ dimer (**Fig. 3A, red**), an additional

observable migration shift may be difficult to observe. Thus, we assume the slowest migrating band is a tetrameric $HigB_2HigA_2$-O1-O2 complex. When the molar ratio of HigB to HigA exceeds one (two HigB monomers to one $HigA_2$ dimer or 1.0 μM HigB for 0.5 μM $HigA_2$ dimer), only free DNA is observed suggesting that excess HigB destabilizes the association between HigA and DNA. These results appear to be similar to what has been observed with other type II TA complexes that exhibit regulation via conditional cooperativity (17, 18, 27).

To determine whether the instability of the HigBHigA complex with O1-O2 is dependent upon the occupancy of both O1 and O2, we next tested complex formation on DNA containing either a scrambled O1 or O2 to prevent $HigA_2$ binding (same mutation as used in Fig. 2). Addition of $HigA_2$ to DNA containing either a scrambled O1 or O2 results in a slower moving species indicative of the $HigA_2$ dimer binding at one operator (**Fig. 3C, orange**). Increasing amounts of HigB shows a single, slower moving molecular weight species (**Fig. 3C, purple**). At this point, we assume the HigBHigA complex is tetrameric ($HigB_2HigA_2$) given the prior crystal structures (26). Once the HigB to HigA molar ratio almost exceeds 1 (i.e. 1.0 μM HigB for 0.5 μM $HigA_2$ dimer), the complex is unstable and DNA is released. Interestingly, in the context of both O1 and O2 (**Fig. 3A**), the molar ratio of HigB to HigA needs to exceed 1 however, when only one operator is available, this release of DNA occurs at slightly less then 1 molar equivalents of HigB and HigA. Therefore, the instability of HigBHigA binding a single operator appears to be accelerated in the absence of an adjacent HigBHigA complex.

Structure of $HigB_2HigA_2$-O2 DNA. To determine how HigBHigA interacts with its operator DNA, we pursued a high-resolution X-ray crystal structure of HigBHigA bound to a single operator, O2. We performed crystallization trials using two HigBHigA constructs: a six histidine (His_6) affinity tag located at the N terminus of HigB and a His_6 affinity tag located at

the C terminus of HigA. Both HigBHigA variants crystallized in the same condition, however, each resulted in a different oligomeric state of the HigBHigA complex bound to O2. The HigBHigA-His_6-O2 complex crystalized in the monoclinic space group C121, was determined to 2.4 Å resolution by single wavelength anomalous diffraction phasing and contained a $HigA_2$ dimer bound to two HigB monomers (**Fig. 4**). The His_6-HigBHigA-O2 complex crystalized in the tetragonal space group $I4_1$, was determined by molecular replacement using the previously determined $HigA_2$ model (PDB code 6CF1) to 2.8 Å resolution and contained a $HigA_2$ dimer bound to a single HigB (**Fig. 5**; **Table S3**). In both structures, residues 1–91 were built for each HigB monomer (92 total residues) and all nucleotides (1–21) were built for the O2 DNA duplex (**Fig. S2**). Residues 1–101 and 1–102 in the $HigB_2HigA_2$ structure and residues 1–91 and 1–95 in the $HigBHigA_2$ structure were modeled (104 total residues) (**Fig. S2**).

The HTH motif in HigA consists of α2, loop 3 and α3 and this region interacts with the major groove of the operator O2 DNA (**Fig. 4A**). In the tetrameric $HigB_2HigA_2$-O2 structure, HigA contacts the $T_{-1,}$ $G_{-2,}$ $T_{-3,}$ A_{-4} O2 sequence on the *hig* negative strand (38) (**Figs. 4A, B**). HigA residue Arg40 interacts with the Hoogsteen face of G_{-2} to make the only sequence-specific protein-DNA contact. Residues Thr34 and Thr37 (from α3) contact the phosphate of G_{+7} while the sidechains of Ser23 (from loop 2), Ser39 (from α3), and Lys45 (from α3) are all within hydrogen bonding distance of nucleotides T_{-7}, A_{-6}, T_{-5}, and T_{-4}, respectively which are located on the opposite DNA strand (**Fig. S3**). Additionally, Ala36 and Thr34 form van der Waals interactions with the nucleobase C5 methyl of A_{-3}. These interactions are similar to those previously observed in the $HigA_2$-O2 DNA interaction (38) and are also present between HigA and O2 on the opposite strand, indicating that HigB binding to form the tetrameric $HigB_2$HigA2-O_2 complex does not change interactions of $HigA_2$ with O2.

The termini of antitoxins are typically intrinsically disordered contributing to their proteolysis during external stimuli. In the free $HigA_2$ structure (38), the N terminus is disordered (**Fig. S4A,B**). Upon HigB binding, the HigA termini becomes ordered both in the free $HigB_2HigA_2$ structure (26) and upon binding DNA ($HigB_2HigA_2$-O2 DNA) (**Fig. 4C; Fig. S4C,D**). The N- and C-termini of HigA form intramolecular interactions in addition to interactions with α1 of an adjacent HigB in the crystal lattice (**Fig. S4A,B**). Specifically, N-terminal residues Arg2 (side chain) and Gln3 (backbone carbonyl) form salt bridges with C-terminal residues Glu80 and Arg77, respectively, and these interactions presumably stabilize the termini. Thus, binding of HigB stabilizes HigA both in the presence or absence of DNA.

Comparison of the overall architecture of $HigB_2HigA_2$-O2 DNA to $HigB_2HigA_2$ (26) or $HigA_2$ (38) reveals subtle changes that may be important for O2 DNA binding and transcriptional repression. Aligning analogous HigA monomers from the $HigB_2HigA_2$-O2 and the $HigB_2HigA_2$ structures (PDB code 4MCX) reveals a ~14° displacement of the adjacent, second HigA protomer (**Fig. 4D**). Similarly, comparison of the free $HigA_2$ dimer (PDB code 6CF1) to $HigB_2HigA_2$-O2 also shows rotation of HigA upon DNA binding, although the movement is not as large as compared to when HigB is present (~8° rotation versus a ~14° rotation) (**Fig. S5**). Thus, $HigA_2$ reorients to bind DNA and HigB binding to a $HigA_2$-DNA complex minimally influences the protein-DNA interface.

Structure of $HigBHigA_2$-O2 DNA. As noted above, both the tetrameric $HigB_2HigA_2$-O2 DNA and trimeric $HigBHigA_2$-O2 DNA crystal forms formed in the same crystallization conditions and resulted in two different macromolecular structures (**Table S3**). Interestingly, not all of the interactions seen in tetrameric $HigB_2HigA_2$-DNA are conserved in the trimeric $HigBHigA_2$-O2 structure. While critical interactions of HigA with the T_{-1}, G_{-2}, T_{-3}, A_{-4} recognition sequence are maintained, α2 and α3 of the HTH DNA-binding motif slightly moves away from O2, no

longer positioning Ser23 and Lys45 to hydrogen bond with the phosphates of T_{-7} and T_{-4} (**Fig. 5B; Fig. S3**).

Global comparison of the $HigB_2HigA_2$-O2 structure with the $HigBHigA_2$-O2 structure reveal only a ~1º difference emphasizing how similar the two structures are (**Fig. 5D**). Likewise there are very little differences in the position of $HigA_2$ bound to O2 (38) in the absence or presence of HigB. Thus, it does not appear that HigB binding influences the position of $HigA_2$ on DNA. It appears the largest structural change results from either $HigA_2$ or $HigB_nHigA_2$ binding to DNA (~14° rotation, where "n" denotes either a single HigB or two HigB monomers; **Fig. 4D**). Previously we described how HigA N-terminal residues Arg2 and Gln3 interact with its C-terminal residues Arg77 and Glu80 in the $HigB_2HigA_2$-O2 structure (**Fig. 4C**). We find that even a single HigB binding can cause these termini residues to become ordered (**Fig. S4E**).

A curious crystallization note for the trimeric $HigBHigA_2$-O2 complex is that there is an adjacent molecule in the neighboring asymmetric unit that overlaps with the missing HigB (**Fig. S6**). This ejection of HigB from the HigBHigA complex is surprising given the known tight interactions of TA complexes where affinities are typically sub-nanomolar (29, 40-42). Therefore, we think it is unlikely that the trimeric $HigBHigA_2$-O2 complex results from crystal packing. Interestingly, the structures of both HigBHigA complexes with the different placement of the His_6 tag were solved and both found to be tetrameric $HigB_2HigA_2$ in the absence of DNA. Taken together, we propose that there is a mixture of both trimeric and tetrameric HigBHigA complexes bound to DNA in solution. We next sought to examine the functional relevance of the trimeric $HigBHigA_2$-O2 complex.

$HigB_2A_2$-O2 and $HigBHigA_2$-O2 complexes exhibit similar dynamics. The structure of the trimeric $HigBHigA_2$-O2 complex is intriguing as most models that describe the

transcriptional regulation of type II TA systems conclude that such an oligomeric state is more stable than the fully loaded complex (18, 21, 42). However, prior to our new structure, there has been no biochemical or direct evidence for the existence of this oligomeric state. To assess the dynamics of both complexes in the presence or absence of O2, we performed molecular dynamics (MD) simulations of four complexes: $HigB_2HigA_2$ and $HigBHigA_2$ in the presence or absence of O2 (**Fig. 6**). The trimeric $HigBHigA_2$ complex in the absence of DNA has not been solved and we generated the model based upon the $HigBHigA_2$-O2 structure. We obtained 1 microsecond-long MD trajectories of each complex and subsequently performed root mean square fluctuation (RMSF) analysis. This analysis reveals overall comparable dynamics: in tetrameric $HigB_2HigA_2$, binding to O2 only marginally affects dynamics, with the largest effects observed at intrinsically flexible regions such as the C termini of HigA monomers (residues 94-102) and loop 3 of HigB (residues 56-62) (**Fig. 6A**). In trimeric $HigBHigA_2$, similar trends are observed, confirming that both oligomeric states represent similarly stable, DNA-bound complexes (**Fig. 6B**). One noted difference is that in the trimeric $HigBHigA_2$-O2 complex, the C-termini of one of the two HigAs is disordered and is not modeled. Two HigB monomers binding causes the C-termini of HigA to regain order but while the C-termini of both HigA monomers can be modeled, this region still exhibits dynamic behavior.

Engineered trimeric $HigBHigA_2$ transcriptionally represses P*hig*. To test whether a trimeric $HigBHigA_2$ complex represses transcription to the same extent as $HigB_2HigA_2$, we attempted to engineer such a variant. Comparison of the $HigB_2HigA_2$ structure with the $HigB_2HigA_2$-O2 DNA structure shows that the two HigB monomers move closer to each other to accommodate binding to DNA (**Fig. 7A**). In particular, HigB loop 5 (L5) located at the interface of the HigB monomers moves ~4Å (**Fig. 4D**). We therefore extended L5 by the

addition of a short, flexible sequence of four residues (Asn, Gly, Asn, Gly (NGNG); called HigB(L5ext)HigA$_2$) to prevent concurrent binding of two HigB monomers to HigA$_2$ (**Fig. 7A**). Expression and purification of HigB(L5ext)HigA$_2$ showed a delayed elution of the complex from the size exclusion column as compared to wild-type HigB$_2$HigA$_2$ (**Fig. 7B**), at a volume corresponding to a molecular weight of 42 kDa (compared to 56 kDa for wild-type HigB$_2$HigA$_2$). The difference in apparent molecular weights indicates that the HigB(L5ext)HigA$_2$ complex is ~14 kDa smaller than the wild-type complex which roughly corresponds to a HigB monomer (molecular weight of ~13 kDa). To assess its thermal stability, we performed nano-differential scanning fluorimetry (nano-DSF) which provides information on the melting temperature (T_m) of the complex. Since this measurement is not at equilibrium, the inflection point is known as T_i. HigB(L5ext)HigA$_2$ is ~5ºC less thermostable than wild-type HigB$_2$HigA$_2$ (60.5ºC vs. 54.0ºC) consistent with an altered oligomeric state (**Fig. 7C**).

To test the ability of the HigB(L5ext)HigA$_2$ variant to repress transcription at *hig*, we performed EMSA and β-gal assays using similar approaches as described above. The HigB(L5ext)HigA$_2$ complex binds to both O1 and O2 DNAs at concentrations similar to wild-type HigB$_2$HigA$_2$ (**Fig. 8A**). Although an intermediate shift is observed (likely representing a HigA$_2$ dimer bound), these data show the trimeric HigB(L5ext)HigA$_2$ interacts with O1 and O2 in a similar manner as wild-type HigB$_2$HigA$_2$. To determine whether the HigB(L5ext)HigA$_2$ complex represses P*hig in vivo*, we used the previously described P*hig* constructs and included a P*hig* containing the HigB(L5ext)HigA$_2$ variant (pQF50-P*hig-higB*(L5ext)*higA-lacZ*; **Fig. 8B; Fig. S7**). As expected, P*hig* alone shows high β-gal activity (normalize to 0% repression) because of the absence of transcriptional repressor HigA. P*hig-higBhigA-lacZ* shows little β-gal activity indicating robust HigA repression at P*hig* (~95% repression). The

348 HigB(L5ext)HigA$_2$ variant shows similar repression as wild-type HigB$_2$HigA$_2$ suggesting
349 there is no difference between a trimeric or tetrameric HigBHigA complex.

350 One possibility that we wanted to explore was whether *hig* is responsive to changing
351 toxin levels *in vivo* considering that toxin overexpression in the *phddoc*, *ccdBccdA* and *relEB*
352 systems can relieve repression (17, 18, 27). For this assay, we used a HigB variant (H54A)
353 that is not catalytically active so cell growth won't be impacted by its expression and we
354 know this variant is expressed as detected by Western blot analysis (34, 43). Further, since
355 the active site of HigB is on the opposite surface from its HigA binding surface (26), this
356 variant should not interfere with HigA binding. Overexpression of HigB(H54A) showed
357 minimal impact on repression of P*hig-higBhigA* indicating free HigB(H54A) is unable to
358 interact with HigB$_2$HigA$_2$ bound at O1 or O2 (97.2% vs. 98.0%; **Fig. 8B**). In the case of the
359 engineered HigB(L5ext)HigA$_2$, excess HigB(H54A) expression also has no effect on
360 repression and does not interfere with HigA-mediated repression (**Fig. 8B**). These data
361 support a model whereby *hig* repression is only relieved by HigA proteolysis.

362

363 **DISCUSSION**

364 The roles of bacterial TA modules have been controversial owing to experimental errors in
365 the construction of *E. coli* TA deletion strains and the ambiguity over what activates toxin
366 expression, antitoxin proteolysis and the release of toxin (10, 44, 45). While these activities
367 are still under debate, the way these modules are transcriptionally autoregulated is known
368 to clearly contribute to their changing expression patterns in response to external stimuli
369 although many outstanding questions still remain (17, 18, 27). One question is how different
370 oligomeric TA complexes influence physical interactions with their DNA operators and the
371 assembly and/ or cooperativity of TA complexes bound at adjacent operator sites. In this
372 study, we focused on the regulation of the *higBhigA* TA module first identified on the

antibiotic-resistance Rts1 plasmid associated with a urinary tract infection caused by *P. vulgaris* (32). Our prior work revealed that while the HigB toxin adopts a canonical ribonuclease fold similar to other members of the RelE family (26), HigA antitoxin suppresses HigB activity in an unusual manner, suggesting that transcriptional repression may also be different. We therefore sought to understand how the *higBhigA* operon is regulated and how its diverse architecture might influence its negative regulation of transcription.

Higher-order oligomeric complexes of the PhDDoc, RelBRelE and CcdBCcdA TA complexes alter their thermodynamic interactions with operators and thus influence transcriptional responsiveness (17, 18, 27). We find that although HigA binding at adjacent operators is not cooperative (38) (**Fig. 2**), the addition of HigB promotes the formation of higher-order complexes and disassembly of the complex does appear to occur once a threshold of excess toxin to antitoxin is reached (**Figs. 2,3**). On the surface, these data appear to be consistent with how other TAs are regulated via the conditional cooperativity model or, as other transcriptional systems are described, as molecular rheostats (14). However, in an attempt to perturb the system *in vivo* by increasing HigB concentrations in the presence of the HigBHigA complex bound at O1 and O2 operators, we find no observable change in repression in contrast to these TA systems (**Fig. 8B**). These conflicting data indicate that the perceived disruption of the higher order HigBHigA-O2 DNA complex via EMSA may not be reflective of transcriptional repression that we observe *in vivo*. Further, these results suggest a different mode of regulation for the *higBhigA* operon.

One hallmark of conditional cooperativity that defines transcriptional regulation of TA operons is that the addition of excess toxin to antitoxins bound at operator sites changes the affinity of these interactions because toxin can act both as a co-repressor and de-repressor (17, 18, 22). In general, when the toxin and antitoxin are expressed at equimolar ratios, the toxin functions as a co-repressor and transcriptional repression is enhanced. Once toxin

concentrations exceed that of the antitoxin, however, disruption of the repressor complex ensues, antitoxin disengages from the promoter, and transcription proceeds (**Fig. 1**). To achieve this mode of regulation, defined oligomeric states of TA complexes have different affinities: for example, although the structure of RelBRelE complex indicates the complex is tetrameric with two RelE toxins and two RelB antitoxins (21), a trimeric version of the complex (two RelBs, one RelE) is proposed to have the highest affinity for the *rel* operon (18, 21). In the presence of a greater excess of toxin, the tetrameric $RelB_2RelE_2$ forms at adjacent operators causing a change from a high affinity to a low affinity state, and the RelBRelE complex no longer binds to DNA (**Fig. 1**). This model permits the system to be responsive to changing levels of toxin but at this point, there is limited biochemical and structural data that corresponds to these changing oligomeric states.

We serendipitously solved two different structures of the HigBHigA-O2 complexes that differ in their molar ratios of HigA antitoxin to the HigB toxin (**Figs. 4,5**). These different oligomeric states capture, for the first time, how both the tetrameric $HigB_2HigA_2$ and trimeric $HigBHigA_2$ interact with O2 to repress transcription. The trimeric $HigBHigA_2$-O2 DNA structure was especially unexpected given that the tetrameric $HigB_2HigA_2$ form predominates in the absence of operator (26). The molecular interactions of each HigBHigA complex with its operator are largely maintained, initially suggesting that different oligomeric states may not contribute to changes in repression for this system. Molecular dynamic simulations of both the trimeric and tetrameric HigBHigA-O2 complexes show each complex have similar dynamics when bound to DNA, offering further support for the ability of both oligomeric states to contribute to repression (**Fig. 6**). Further, engineering of a forced trimeric $HigBHigA_2$ oligomeric complex revealed similar levels of transcriptional repression (**Figs. 7,8; Fig. S7**). Together, these data support a model where *hig* is regulated as a simple on/off switch

422 incalcitrant to changing levels of toxin and influenced solely by HigA proteolysis likely as
423 result of the Rts1 plasmid not being inherited.

424 There are several other reasons for why *hig* may be regulated in a different manner
425 from other TA operons. In TA operons regulated as molecular rheostats including *phddoc*,
426 *relBrelE* and *ccdBccdA*, a single promoter controls expression of the operon and the
427 antitoxin is encoded first (17, 18, 22). It has been suggested this operon organization allows
428 for the antitoxin to be expressed in excess of the toxin, which is required to suppress toxicity
429 when the system is transcriptionally de-repressed (46, 47). In *hig*, there is a second weak
430 promoter, P*higA*, that allows for independent expression of HigA to ensure excess HigA is
431 always present to suppress HigB (48). It is not clear if this change in operon organization
432 accounts for why *hig* is regulated via a simple on/off switch but other TA operons such as
433 *mqsRA* that also have this reverse architecture and contain multiple promoters do not appear
434 to be regulated via conditional cooperativity (29). In contrast, the DinJ-YafQ TA module does
435 not have this reverse architecture but does not appear to be regulated by conditional
436 cooperativity (30). Therefore, there must be some other currently unappreciated mechanism
437 by which this TA system balances antitoxin expression for its regulation.

438 The results presented here provide new insight into the transcriptional regulation of
439 the plasmid-associated *hig* operon and add to the growing diversity of mechanisms used to
440 balance transcriptional responses of these abundant bacterial gene pairs. In the future,
441 additional biophysical studies are needed to reconcile the role of changing macromolecular
442 complex formation in the regulation of TA pairs and to align these properties with
443 transcriptional responsiveness.

444

445 **MATERIALS AND METHODS**

446 **Strains and plasmids**. *E. coli* BL21(DE3) cells were used for expression of His_6-HigA, His_6-
447 HigBHigA and HigBHigA-His_6 proteins from pET28a, pET28a and pET21c vectors,
448 respectively as previously reported (26). *E. coli* BW25113 cells were used for all β-gal
449 experiments and HigB(H54A)-His_6 expression (49). All point mutations were introduced by
450 site-directed mutagenesis and sequences were verified by DNA sequencing (Genewiz).
451
452 **HigA, HigB and HigBHigA expression and purification.** The His_6-HigA, His_6-HigBHigA
453 and HigBHigA-His_6 protein complexes were overexpressed and purified as previously
454 described with minor modifications (26). These differences included incubation of His_6-HigA
455 at 18°C overnight after protein induction and removal of the His_6 tag from His_6-HigA and His_6-
456 HigBHigA with thrombin prior to gel filtration chromatography. HigB(H54A) protein was
457 overexpressed and purified as previously described (43).
458
459 **Electrophoretic mobility shift assays (EMSAs).** To construct the dsDNA for the EMSA,
460 pairs of complementary single-stranded oligonucleotides were diluted to 2 μM each in 100
461 mM NaCl, 10 mM Tris-HCl pH8. The O1-O2, O1-O2(scrambled) or O1(scrambled)-O2
462 oligonucleotide mixtures (**Table S1**) of the *hig* promoter fragment were incubated in boiling
463 water and then cooled at room temperature overnight. The dsDNA oligos were diluted to 150
464 nM in EMSA binding buffer (100 mM NaCl, 10 mM $MgCl_2$, 5% glycerol, 0.01 mg/mL bovine
465 serum albumin). Purified wild-type HigA, HigBHigA, and HigB(L5ext)HigA proteins were
466 diluted to 10 μM in EMSA binding buffer and serially diluted to give a series of protein
467 concentrations ranging from 25 nM to 0.8 μM. The binding reactions were incubated on ice
468 for 20 min and 10 μL of each reaction was loaded onto 8% native, polyacrylamide-0.5X
469 TBE/10% glycerol gels (50 mM Tris-HCl pH 8, 50 mM boric acid, 5 mM EDTA, 10% glycerol)
470 and subjected to electrophoresis at 110 V limiting on ice for 60 min. To visualize the DNA

and DNA-protein complexes, the gels were stained with SYBR green nucleic acid gel stain (ThermoFisher Scientific) in 0.5X TBE/10% glycerol for 30 min with gentle agitation and then the fluorescence was imaged with a Typhoon Trio phosphoimager (GE Healthcare; 488 nm excitation and 526 nm emission). Assays were performed in duplicate with representative gels shown. Band intensities for both free and bound *hig* DNA were quantified with ImageQuant 1D gel analysis software using the rolling ball background subtraction. For HigA or HigBHigA bound to either O1 or O2, the binding data were fit using a one site-specific binding equation (Y (specific binding , μM) = Bmax * X / [K_D + X]) in GraphPad Prism 9.0.0.

Crystallization, data collection and structure determination of the HigBHigA-O2 DNA complexes. The complex was formed by mixing either His_6-HigBHigA or selenomethionine-derivatized HigBHigA-His_6 (both in 40 mM Tris-HCl, pH 7.5, 250 mM KCl, 5 mM $MgCl_2$, and 5 mM β-mercaptoethanol) with O2 operator DNA (10 mM Tris, pH 8, 100 mM NaCl, and 1 mM EDTA) at one $HigB_2HigA_2$ tetramer to one O2 dsDNA molar ratio. The complexes were diluted to 5.95 mg/mL HigBHigA and 1.55 mg/mL O2 DNA by the addition of buffer (20 mM Tris, pH 8, 10 mM $MgCl_2$, and 100 mM NaCl). Crystals of HigBHigA bound to O2 DNA were grown by sitting drop vapor diffusion and crystallized in 0.2 M $CaCl_2$ and 10-25% (w/v) polyethylene glycol 3,350 at 20°C. Both crystal forms grew after two days and were cryoprotected by serially increasing the concentration of ethylene glycol in the mother liquor from 10-30% (w/v) followed by flash freezing in liquid nitrogen.

Two X-ray datasets were collected at the Northeastern Collaborative Access Team (NE-CAT) 24-ID-C and Southeast Regional Collaborative Access Team (SER-CAT) 22-ID facilities at the Advanced Photon Source (APS) at the Argonne National Laboratory. For the tetrameric $HigB_2HigA_2$-O2 complex, 360° of data (0.5° oscillations) were collected on a PILATUS 6M-F detector (DECTRIS Ltd., Switzerland) using 0.9792 Å radiation. For the

trimeric HigBHigA$_2$-O2 complex, 90° of data (0.5° oscillations) were collected on a MARMOSAIC 300 mm CCD detector (Rayonix, L.L.C., USA) using 1.0 Å radiation. XDS was used to integrate and scale the data (50). The tetrameric HigB$_2$HigA$_2$-O2 structure was solved by single wavelength anomalous diffraction phasing using AutoSol from the PHENIX software suite (51) and thirteen heavy atom sites were found. The trimeric HigBHigA$_2$-O2 structure was solved using the structure of the HigA$_2$ dimer (PDB code 6CF1) as a molecular replacement search model in the PHENIX software suite. XYZ coordinates, real space, and B-factors (isotropic) were refined iteratively in PHENIX and model building was performed using the program Coot (52). Final refinement of the structures gave crystallographic R_{work}/R_{free} of 17.6/21.8% for trimeric HigBHigA$_2$-O2 and 17.5/22.1% for tetrameric HigB$_2$HigA$_2$-O2. All figures were created in PyMol (53).

β-galactosidase assays. The *hig* operon was chemically synthesized (IDT), digested and ligated into a pQF50 vector with *lacZ* downstream (pQF50-*hig* constructs). *E. coli* BW25113 transformed with pQF50-*hig* variants or pBAD33-*higB*(H54A) were used for all experiments. Two methods were used to perform β-gal assays. The first set of β-gal assays presented herein (with constructs containing wild-type versus mutated operators) were performed using the PopCulture® Reagent based method (54). All overnight cultures were grown in M9 minimal media supplemented with 0.2% glucose, 1 M $MgSO_4$, 1 M $CaCl_2$, and 10% casamino acids. Subsequent experiments were performed with M9 minimal media supplemented with 20% glycerol instead of glucose. OD_{600} was measured hourly until an OD_{600} of 0.2 was reached, arabinose was added to a final concentration of 0.2%, and further incubated for 4 hrs. 1 mL aliquots were pelleted, resuspended in 500 µL of M9 media and diluted to an OD_{600} of 0.5 in M9 media. 80 µL were transferred to 96-well plate and 120 µL of freshly mixed β-gal reagent (60 mM Na_2SO_4, 40 mM NaH_2PO_4, 10 mM KCl, 1 mM $MgSO_4$, 36 mM β-me, 166

μL/mL T7 lysozyme, 1.1 mg/mL ortho-Nitrophenyl-β-galactoside and 6.7% PopCulture® Reagent (Millipore-Sigma)) was added to each well. 80 μL of M9 media was also added to wells containing 120 μL of β-gal reagent as a negative control. The microplate was read by a Biotek Cytation 5 multi-mode reader pre-incubated at 30°C, with OD_{600} and OD_{420} measurements taken every 5 min for 1 hr with agitation.

The second set of β-gal assays presented herein (in the absence or presence of HigB(H54A)) were performed using a method previously described (38). In both approaches, activity in Miller Units (M.U.) was measured using the formula: total activity (M.U.) = (1000*OD_{420}) / (OD_{600} * volume of culture used (mL) * 0.5). Assays were performed in triplicate with two technical replicates.

Differential scanning fluorimetry (DSF). The thermal stability of wild-type HigBHigA and HigB(L5ext)HigA were assessed using a Tycho NT.6 instrument (NanoTemper). Protein was heated at 0.1ºC steps over a temperature range of 35ºC to 95ºC, during which intrinsic fluorescence at 350 and 330 nm was measured. Inflection temperature (T_i) was determined for each apparent unfolding transition from the temperature-dependent change in the ratio of 350 and 330 nm measurements. Assays were performed in triplicates.

Molecular dynamics simulations. Starting models for molecular dynamics (MD) simulations were prepared from PDB codes 6W6U ($HigB_2HigA_2$-O2) and 6WFP ($HigBHigA_2$-O2). Simulations were performed on the tetrameric or trimeric HigBHigA structures in the absence or presence of O2 DNA ($HigB_2HigA_2$-O2, $HigBHigA_2$-O2, $HigB_2HigA_2$ and $HigBHigA_2$). All complexes were prepared using the Xleap module of AmberTools 18 (55), the ff14SB forcefield for protein atoms (56) and the OL15 forcefield (57) for DNA. Complexes were solvated in an octahedral box of TIP3P water (58) with a 10 Å buffer. Ions were added

to each complex to achieve a final concentration of 150 mM NaCl. Minimization was performed in three rounds, each employing steepest descent (5000 steps) followed by conjugate gradient (5000 steps). In the first round, restraints of 500 kcal/mol-Å^2 were applied to all solute atoms. In the second round, solute restraints were reduced to 100 kcal/mol-Å^2. All restraints were removed in the third round. Complexes were heated from 0 to 300 K with a 100-ps run with constant volume periodic boundaries and restraints of 10-kcal/mol-Å^2 on solute atoms. All MD simulations were performed using AMBER2018 (55, 59, 60). Two stages of equilibration were performed: 10 ns MD in the NPT ensemble with 10-kcal/mol-Å^2 restraints on solute atoms, followed by an additional 10 ns MD run with restraints reduced to 1 kcal/mol-Å^2. Finally all restraints were removed and 1 microsecond production simulations obtained for each complex. Long-range electrostatics were evaluated with a cutoff of 10 Å and all heavy atom-hydrogen bonds were fixed with the SHAKE algorithm (61). Following MD, the CPPTRAJ module (62) of AmberTools 18 was used to calculate root mean square fluctuations (RMSF) of each protein reside in each complex.

ACKNOWLEDGEMENTS

Research reported in this publication was partially supported by a National Science Foundation CAREER award MCB 0953714 (CMD), a NIH Biochemistry, Cellular and Molecular Biology Graduate Training Grant 5T32GM8367 (MAS), and NIH NRSA F31 Fellowship GM108351 (MAS) and a Burroughs Wellcome Fund Investigator in the Pathogenesis of Infectious Disease award (CMD). We thank F. M. Murphy IV and staff members of the NE-CAT beamlines for assistance during data collection and G. L. Conn and other Dunham lab members for critical reading of the manuscript. This work is based upon research conducted at the Northeastern Collaborative Access Team beamlines, which are funded by the National Institute of General Medical Sciences from the National Institutes

of Health (P30 GM124165). Additional data were collected at the Southeast Regional Collaborative Access Team (SER-CAT) 22-ID (or 22-BM) beamline at the Advanced Photon Source, Argonne National Laboratory. SER-CAT is supported by its member institutions (www.ser-cat.org/members.html) and equipment grants (S10RR25528 and S10RR028976) from the National Institutes of Health. Use of the Advanced Photon Source was supported by the U. S. Department of Energy, Office of Science, Office of Basic Energy Sciences, under Contract No. DE-AC02-06CH11357.

REFERENCES

1. D. P. Pandey, K. Gerdes, Toxin-antitoxin loci are highly abundant in free-living but lost from host-associated prokaryotes. *Nucleic Acids Res* **33**, 966-976 (2005).
2. K. S. Makarova, Y. I. Wolf, E. V. Koonin, Comprehensive comparative-genomic analysis of type 2 toxin-antitoxin systems and related mobile stress response systems in prokaryotes. *Biol Direct* **4**, 19 (2009).
3. R. Leplae *et al.*, Diversity of bacterial type II toxin-antitoxin systems: a comprehensive search and functional analysis of novel families. *Nucleic Acids Res* **39**, 5513-5525 (2011).
4. H. Karoui, F. Bex, P. Dreze, M. Couturier, Ham22, a mini-F mutation which is lethal to host cell and promotes recA-dependent induction of lambdoid prophage. *EMBO J* **2**, 1863-1868 (1983).
5. T. Ogura, S. Hiraga, Mini-F plasmid genes that couple host cell division to plasmid proliferation. *Proc Natl Acad Sci U S A* **80**, 4784-4788 (1983).
6. K. Gerdes, P. B. Rasmussen, S. Molin, Unique type of plasmid maintenance function: postsegregational killing of plasmid-free cells. *Proc Natl Acad Sci U S A* **83**, 3116-3120 (1986).

7. A. Bravo, G. de Torrontegui, R. Diaz, Identification of components of a new stability system of plasmid R1, ParD, that is close to the origin of replication of this plasmid. *Mol Gen Genet* **210**, 101-110 (1987).
8. S. Tsuchimoto, H. Ohtsubo, E. Ohtsubo, Two genes, pemK and pemI, responsible for stable maintenance of resistance plasmid R100. *J Bacteriol* **170**, 1461-1466 (1988).
9. H. Lehnherr, E. Maguin, S. Jafri, M. B. Yarmolinsky, Plasmid addiction genes of bacteriophage P1: doc, which causes cell death on curing of prophage, and phd, which prevents host death when prophage is retained. *Journal of molecular biology* **233**, 414-428 (1993).
10. N. Fraikin, F. Goormaghtigh, L. Van Melderen, Type II Toxin-Antitoxin Systems: Evolution and Revolutions. *J Bacteriol* **202** (2020).
11. R. Loris, A. Garcia-Pino, Disorder- and dynamics-based regulatory mechanisms in toxin-antitoxin modules. *Chemical reviews* **114**, 6933-6947 (2014).
12. R. Page, W. Peti, Toxin-antitoxin systems in bacterial growth arrest and persistence. *Nat Chem Biol* **12**, 208-214 (2016).
13. F. M. Rossi, A. M. Kringstein, A. Spicher, O. M. Guicherit, H. M. Blau, Transcriptional control: rheostat converted to on/off switch. *Mol Cell* **6**, 723-728 (2000).
14. E. Batchelor, T. J. Silhavy, M. Goulian, Continuous control in bacterial regulatory circuits. *J Bacteriol* **186**, 7618-7625 (2004).
15. M. Gotfredsen, K. Gerdes, The Escherichia coli relBE genes belong to a new toxin-antitoxin gene family. *Mol Microbiol* **29**, 1065-1076 (1998).
16. R. Magnuson, M. B. Yarmolinsky, Corepression of the P1 addiction operon by Phd and Doc. *J Bacteriol* **180**, 6342-6351 (1998).
17. H. Afif, N. Allali, M. Couturier, L. Van Melderen, The ratio between CcdA and CcdB modulates the transcriptional repression of the ccd poison-antidote system. *Mol Microbiol* **41**, 73-82 (2001).

18. M. Overgaard, J. Borch, M. G. Jorgensen, K. Gerdes, Messenger RNA interferase RelE controls relBE transcription by conditional cooperativity. *Mol Microbiol* **69**, 841-857 (2008).

19. A. Harms, D. E. Brodersen, N. Mitarai, K. Gerdes, Toxins, Targets, and Triggers: An Overview of Toxin-Antitoxin Biology. *Mol Cell* **70**, 768-784 (2018).

20. T. Madl *et al.*, Structural basis for nucleic acid and toxin recognition of the bacterial antitoxin CcdA. *Journal of molecular biology* **364**, 170-185 (2006).

21. A. Boggild *et al.*, The crystal structure of the intact E. coli RelBE toxin-antitoxin complex provides the structural basis for conditional cooperativity. *Structure* **20**, 1641-1648 (2012).

22. A. Garcia-Pino *et al.*, Allostery and intrinsic disorder mediate transcription regulation by conditional cooperativity. *Cell* **142**, 101-111 (2010).

23. C. Dienemann, A. Boggild, K. S. Winther, K. Gerdes, D. E. Brodersen, Crystal structure of the VapBC toxin-antitoxin complex from Shigella flexneri reveals a hetero-octameric DNA-binding assembly. *Journal of molecular biology* **414**, 713-722 (2011).

24. B. L. Brown *et al.*, Three dimensional structure of the MqsR:MqsA complex: a novel TA pair comprised of a toxin homologous to RelE and an antitoxin with unique properties. *PLoS Pathog* **5**, e1000706 (2009).

25. M. A. Schumacher *et al.*, Molecular mechanisms of HipA-mediated multidrug tolerance and its neutralization by HipB. *Science* **323**, 396-401 (2009).

26. M. A. Schureck *et al.*, Structure of the Proteus vulgaris HigB-(HigA)2-HigB toxin-antitoxin complex. *J Biol Chem* **289**, 1060-1070 (2014).

27. R. Magnuson, H. Lehnherr, G. Mukhopadhyay, M. B. Yarmolinsky, Autoregulation of the plasmid addiction operon of bacteriophage P1. *J Biol Chem* **271**, 18705-18710 (1996).

28. I. Brzozowska, U. Zielenkiewicz, Regulation of toxin-antitoxin systems by proteolysis. *Plasmid* **70**, 33-41 (2013).

29. B. L. Brown, D. M. Lord, S. Grigoriu, W. Peti, R. Page, The Escherichia coli toxin MqsR destabilizes the transcriptional repression complex formed between the antitoxin MqsA and the mqsRA operon promoter. *J Biol Chem* **288**, 1286-1294 (2013).

30. A. Ruangprasert *et al.*, Mechanisms of toxin inhibition and transcriptional repression by Escherichia coli DinJ-YafQ. *J Biol Chem* **289**, 20559-20569 (2014).

31. Y. Terawaki, H. Takayasu, T. Akiba, Thermosensitive replication of a kanamycin resistance factor. *J Bacteriol* **94**, 687-690 (1967).

32. Q. B. Tian, M. Ohnishi, A. Tabuchi, Y. Terawaki, A new plasmid-encoded proteic killer gene system: cloning, sequencing, and analyzing hig locus of plasmid Rts1. *Biochem Biophys Res Commun* **220**, 280-284 (1996).

33. J. M. Hurley, N. A. Woychik, Bacterial toxin HigB associates with ribosomes and mediates translation-dependent mRNA cleavage at A-rich sites. *J Biol Chem* **284**, 18605-18613 (2009).

34. M. A. Schureck, J. A. Dunkle, T. Maehigashi, S. J. Miles, C. M. Dunham, Defining the mRNA recognition signature of a bacterial toxin protein. *Proc Natl Acad Sci U S A* **112**, 13862-13867 (2015).

35. M. A. Schureck, T. Maehigashi, S. J. Miles, J. Marquez, C. M. Dunham, mRNA bound to the 30S subunit is a HigB toxin substrate. *RNA* **22**, 1261-1270 (2016).

36. S. Hadzi *et al.*, Ribosome-dependent Vibrio cholerae mRNAse HigB2 is regulated by a beta-strand sliding mechanism. *Nucleic Acids Res* **45**, 4972-4983 (2017).

37. B. S. Xu *et al.*, Conformational changes of antitoxin HigA from Escherichia coli str. K-12 upon binding of its cognate toxin HigB reveal a new regulation mechanism in toxin-antitoxin systems. *Biochem Biophys Res Commun* **514**, 37-43 (2019).

38. M. A. Schureck *et al.*, Structural basis of transcriptional regulation by the HigA antitoxin. *Mol Microbiol* **111**, 1449-1462 (2019).

39. Q. B. Tian *et al.*, Specific protein-DNA and protein-protein interaction in the hig gene system, a plasmid-borne proteic killer gene system of plasmid Rts1. *Plasmid* **45**, 63-74 (2001).

40. M. H. Dao-Thi *et al.*, Molecular basis of gyrase poisoning by the addiction toxin CcdB. *Journal of molecular biology* **348**, 1091-1102 (2005).

673 41. S. K. Khoo *et al.*, Molecular and structural characterization of the PezAT chromosomal toxin-
674 antitoxin system of the human pathogen Streptococcus pneumoniae. *J Biol Chem* **282**,
675 19606-19618 (2007).
676 42. M. Overgaard, J. Borch, K. Gerdes, RelB and RelE of Escherichia coli form a tight complex
677 that represses transcription via the ribbon-helix-helix motif in RelB. *Journal of molecular*
678 *biology* **394**, 183-196 (2009).
679 43. M. A. Schureck, A. Repack, S. J. Miles, J. Marquez, C. M. Dunham, Mechanism of
680 endonuclease cleavage by the HigB toxin. *Nucleic Acids Res* **44**, 7944-7953 (2016).
681 44. A. Harms, C. Fino, M. A. Sorensen, S. Semsey, K. Gerdes, Prophages and Growth Dynamics
682 Confound Experimental Results with Antibiotic-Tolerant Persister Cells. *mBio* **8** (2017).
683 45. F. Goormaghtigh *et al.*, Reassessing the Role of Type II Toxin-Antitoxin Systems in Formation
684 of Escherichia coli Type II Persister Cells. *mBio* **9** (2018).
685 46. W. T. Chan, M. Espinosa, C. C. Yeo, Keeping the Wolves at Bay: Antitoxins of Prokaryotic
686 Type II Toxin-Antitoxin Systems. *Front Mol Biosci* **3**, 9 (2016).
687 47. H. S. Deter, R. V. Jensen, W. H. Mather, N. C. Butzin, Mechanisms for Differential Protein
688 Production in Toxin-Antitoxin Systems. *Toxins* **9** (2017).
689 48. Q. B. Tian, T. Hayashi, T. Murata, Y. Terawaki, Gene product identification and promoter
690 analysis of hig locus of plasmid Rts1. *Biochem Biophys Res Commun* **225**, 679-684 (1996).
691 49. K. A. Datsenko, B. L. Wanner, One-step inactivation of chromosomal genes in Escherichia
692 coli K-12 using PCR products. *Proc Natl Acad Sci U S A* **97**, 6640-6645 (2000).
693 50. W. Kabsch, Xds. *Acta crystallographica* **66**, 125-132 (2010).
694 51. P. D. Adams *et al.*, PHENIX: a comprehensive Python-based system for macromolecular
695 structure solution. *Acta crystallographica* **66**, 213-221 (2010).
696 52. P. Emsley, B. Lohkamp, W. G. Scott, K. Cowtan, Features and development of Coot. *Acta*
697 *crystallographica* **66**, 486-501 (2010).
698 53. Schrodinger, LLC (2010) The PyMOL Molecular Graphics System, Version 1.3r1.

699 54. J. Schaefer, G. Jovanovic, I. Kotta-Loizou, M. Buck, Single-step method for beta-
700 galactosidase assays in Escherichia coli using a 96-well microplate reader. *Anal Biochem*
701 **503**, 56-57 (2016).
702 55. I. Y. B.-S. D.A. Case, S.R. Brozell, D.S. Cerutti, T.E. Cheatham, III, V.W.D. Cruzeiro, T.A.
703 Darden, R.E. Duke, D. Ghoreishi, M.K. Gilson, H. Gohlke, A.W. Goetz, D. Greene, R Harris,
704 N. Homeyer, Y. Huang, S. Izadi, A. Kovalenko, T. Kurtzman, T.S. Lee, S. LeGrand, P. Li, C.
705 Lin, J. Liu, T. Luchko, R. Luo, D.J. Mermelstein, K.M. Merz, Y. Miao, G. Monard, C. Nguyen,
706 H. Nguyen, I. Omelyan, A. Onufriev, F. Pan, R. Qi, D.R. Roe, A. Roitberg, C. Sagui, S. Schott-
707 Verdugo, J. Shen, C.L. Simmerling, J. Smith, R. SalomonFerrer, J. Swails, R.C. Walker, J.
708 Wang, H. Wei, R.M. Wolf, X. Wu, L. Xiao, D.M. York and P.A. Kollman (2018) AMBER 2018.
709 (University of California, San Francisco).
710 56. J. A. Maier *et al.*, ff14SB: Improving the Accuracy of Protein Side Chain and Backbone
711 Parameters from ff99SB. *J Chem Theory Comput* **11**, 3696-3713 (2015).
712 57. R. Galindo-Murillo *et al.*, Assessing the Current State of Amber Force Field Modifications for
713 DNA. *J Chem Theory Comput* **12**, 4114-4127 (2016).
714 58. W. L. Jorgensen, J. Chandrasekhar, J. D. Madura, R. W. Impey, M. L. Klein, Comparison of
715 simple potential functions for simulating liquid water. *J. Chem. Phys.* **79** (1983).
716 59. R. Salomon-Ferrer, A. W. Gotz, D. Poole, S. Le Grand, R. C. Walker, Routine Microsecond
717 Molecular Dynamics Simulations with AMBER on GPUs. 2. Explicit Solvent Particle Mesh
718 Ewald. *J Chem Theory Comput* **9**, 3878-3888 (2013).
719 60. S. Le Grand, A. W. Gotz, R. C. Walker, SPFP: Speed without compromise—A mixed
720 precision model for GPU accelerated molecular dynamics simulations. *Computer Physics*
721 *Communications* **184**, 374-380 (2013).
722 61. J. C. Ryckaert, G.; Berendsen, H.J.C., Numerical integration of the cartesian equations of
723 motion of a system with constraints: molecular dynamics of n-alkanes. *Journal of*
724 *Computational Physics* **23**, 327-341 (1977).

62. D. R. Roe, T. E. Cheatham, 3rd, PTRAJ and CPPTRAJ: Software for Processing and Analysis of Molecular Dynamics Trajectory Data. *J Chem Theory Comput* **9**, 3084-3095 (2013).

FIGURES

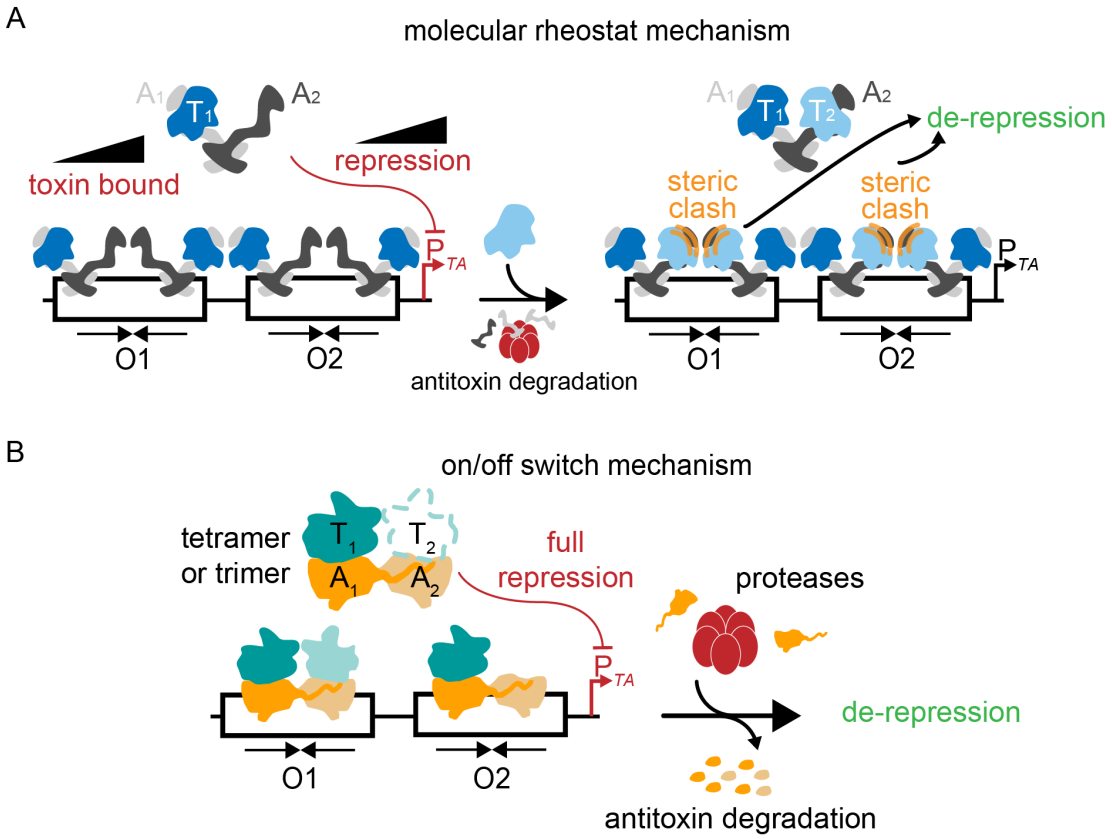

Figure 1. Diverse transcriptional control mechanisms that regulate expression of toxin-antitoxin complexes. Toxin (T) and antitoxin (A) proteins form multimeric complexes that bind operator sites (O1 and O2) that overlap with their promoters (P_{TA}) to repress transcription. (**A**) In some type II toxin-antitoxin systems, changing levels of toxins (due to antitoxin proteolysis) that bind to the repressor complex leads to steric clashes and/or changes in affinity causing de-repression. In this case, the system functions as a molecular rheostat responsive to toxin levels. (**B**) In contrast, other toxin-antitoxin systems are not sensitive to changes in toxin concentrations and thus function as on/off transcriptional switches dependent on antitoxin depletion from proteolysis.

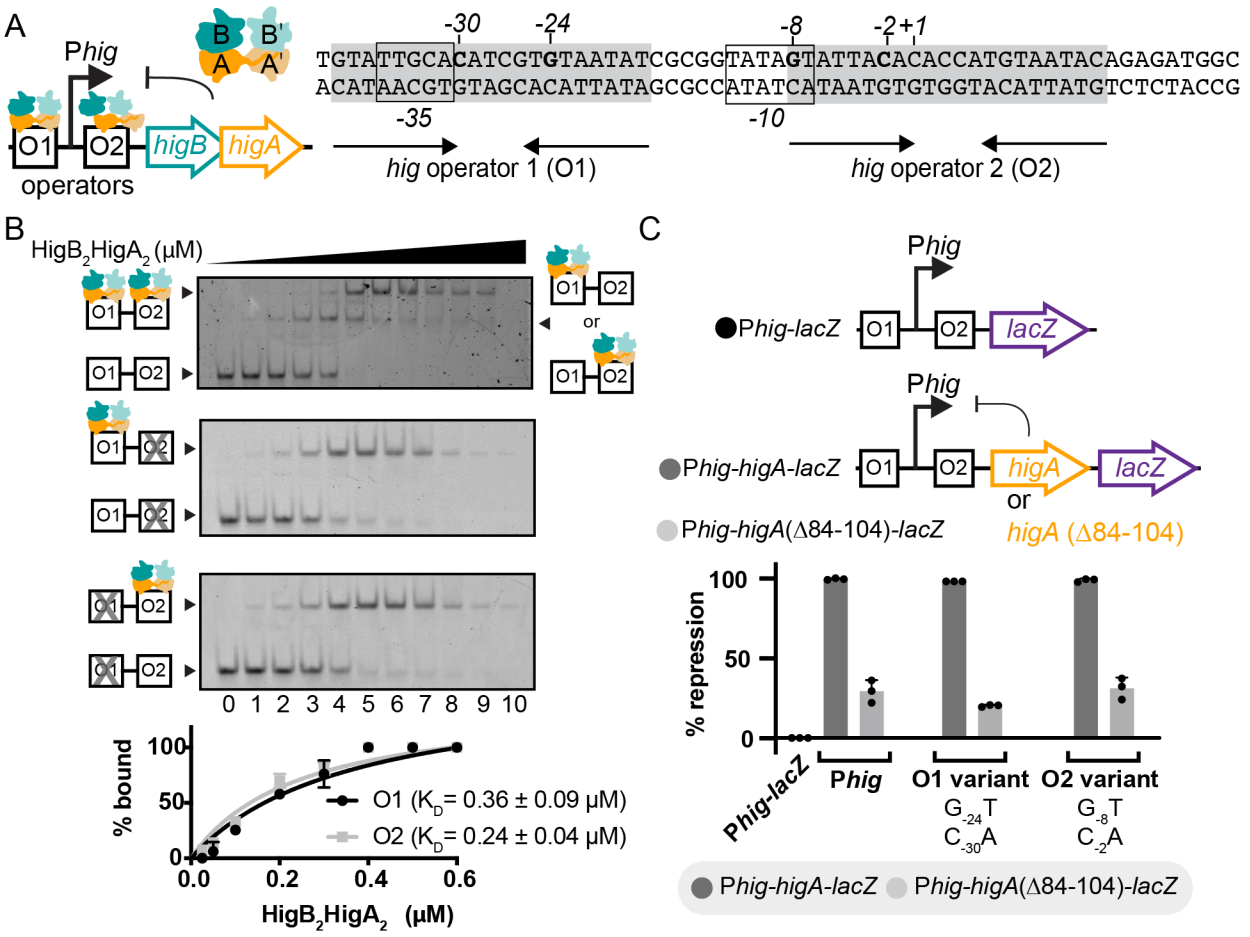

Figure 2. Binding of $HigB_2HigA_2$ to a single operator is sufficient for transcriptional repression of the *hig* operon. (**A**) *Left*, organization of the *hig* operon containing the operators O1 and O2, the P*hig* promoter, *higB* toxin and *higA* antitoxin genes. *Right*, the nucleotide sequences of O1 and O2, with the +1 transcriptional start site and the -35 and -10 sites indicated. The sequence recognized by HigA is shown in grey and operator nucleotides C_{-30}, G_{-24}, G_{-8}, and C_{-2} important for HigA binding are shown in bold. (**B**) EMSA of $HigB_2HigA_2$ binding to wild-type P*hig* (top), O1 only (O2 scrambled; middle), and O2 only (O1 scrambled; bottom) DNA. Band intensities were plotted from EMSAs as the percent of $HigB_2HigA_2$ bound to DNA versus $HigB_2HigA_2$ (concentrations used: 0, 0.025, 0.05, 0.1, 0.2, 0.3, 0.4, 0.5, 0.6, 0.7, 0.8 μM). Curves represent the fit from which K_Ds were calculated. (**C**) β-gal assays of *E. coli* BW25113 transformed with pQF50-P*hig-lacZ* (black), pQF50-P*hig-*

775 *higA-lacZ* (dark grey), or pQF50-P*hig-higA*(Δ84-104)-*lacZ* (light grey). Each operator site
776 was tested using known operator mutations of either O1 ($G_{-24}T$, $C_{-30}A$) or O2 ($G_{-7}T$, $C_{-2}A$)
777 (38).
778
779
780
781
782
783
784
785
786
787
788
789
790
791
792
793
794
795
796
797
798
799

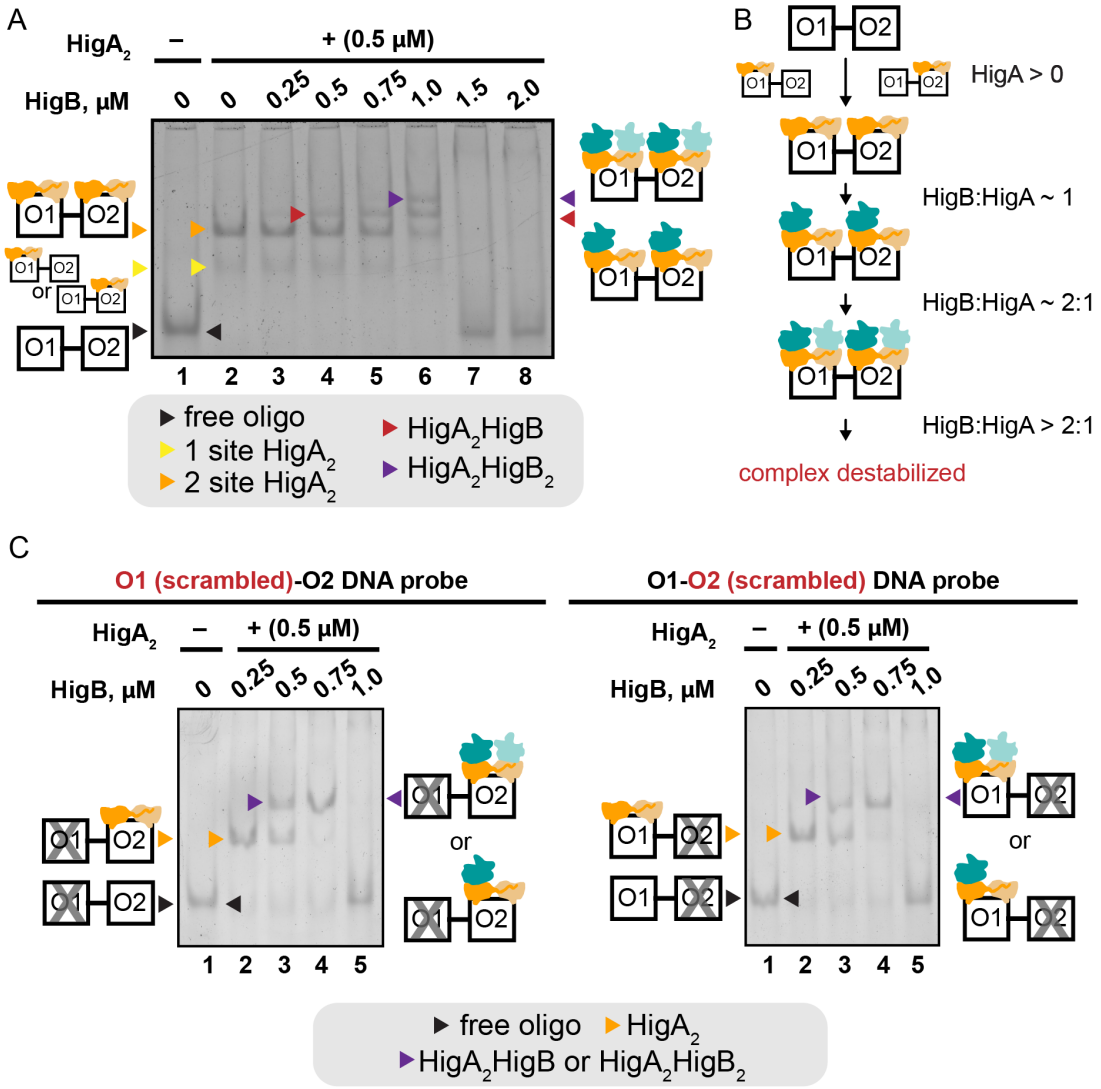

Figure 3. Formation of higher oligomeric states upon addition of HigB to the HigA-DNA complex. (**A**) EMSA of HigB addition to the $HigA_2$-O1-O2 DNA complex. The O1-O2 DNA migrates the fastest (lane 1, black arrowhead) and incubation with the 0.5 μM $HigA_2$ dimer results in a retardation of O1-O2 to form two shifts (lane 2, yellow and orange arrowheads). Increasing amounts of HigB results in the formation of higher molecular weight complexes (lanes 3-6, red and purple arrowheads). When the molar ratio of HigB to HigA exceeds 1 (>1.0 μM HigB for 0.5 μM $HigA_2$ dimer), the high molecular weight shifts are no longer observed indicating that neither HigA nor HigB binds. (**B**) Schematic of the different

809 HigBHigA-O1-O2 DNA complexes formed with changing the HigB:HigA ratio. Multiple
810 oligomeric arrangements are possible in the case of a trimeric $HigA_2HigB$ complex but only
811 one example is shown. (**C**) EMSA of HigB addition to the $HigA_2$-O1-O2 DNA complex when
812 either O1 or O2 is scrambled. O1-O2 DNA migrates the fastest (lane 1, black arrowhead)
813 and incubation with the $HigA_2$ dimer results in a retardation of O1-O2 to form two shifts (lane
814 2, orange arrowhead). The addition of HigB results in the formation of higher molecular
815 weight complexes (lane 3, purple arrowhead) with a molar excess of HigB over HigA causes
816 the scrambled DNA probe to be released (lane 5).
817
818
819
820
821
822
823
824
825
826
827
828
829
830
831
832
833

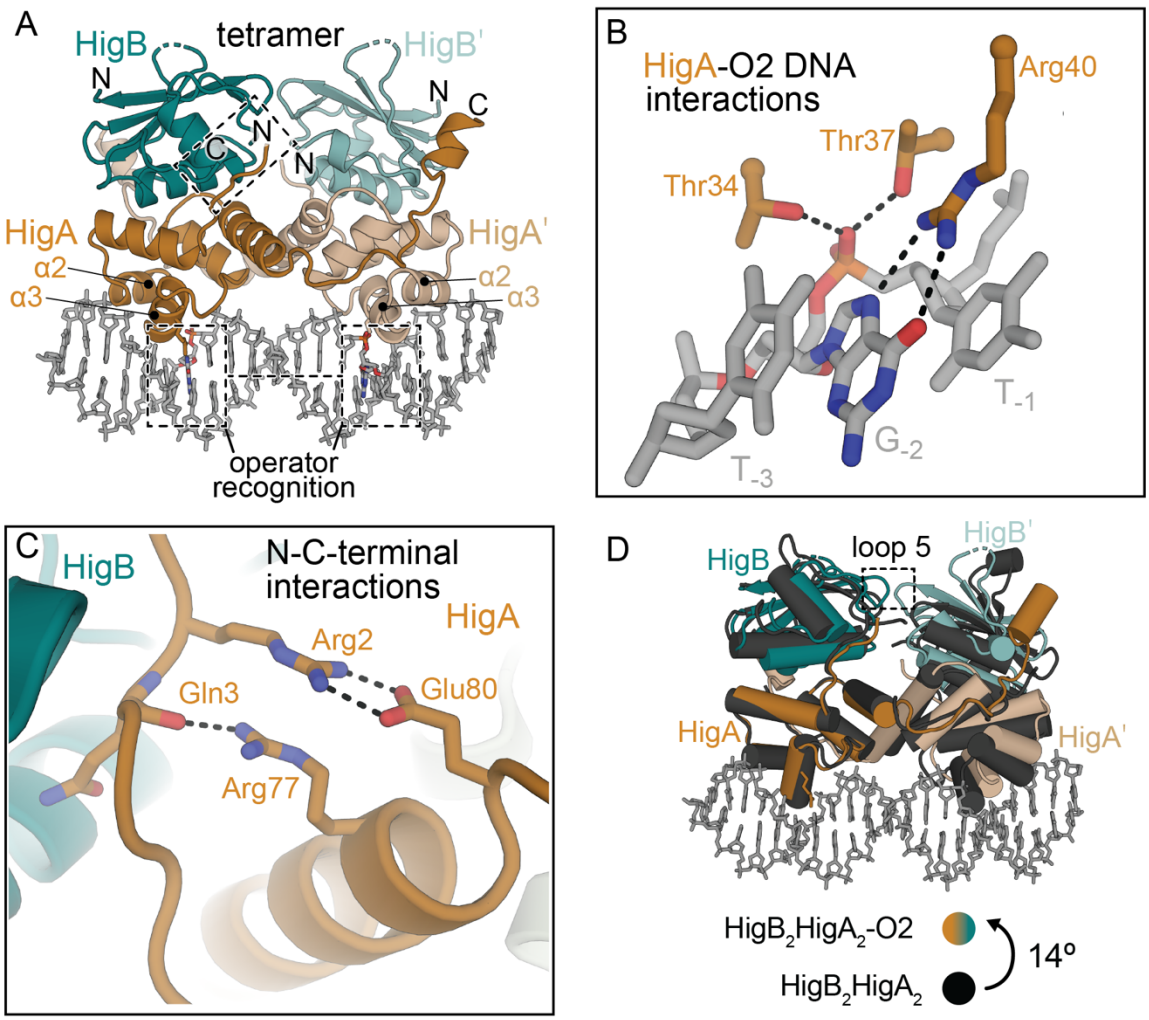

Figure 4. Structure of tetrameric $HigB_2HigA_2$ bound to O2 DNA. (**A**) The 2.4-Å structure of tetrameric $HigB_2HigA_2$-O2 DNA complex (PDB code 6W6U). HigA recognizes the T_{-1}, G_{-2}, T_{-3}, A_{-4} DNA operator region via α2 and α3. N and C-terminal regions of HigA are boxed. (**B**) HigA Arg40 makes the only sequence specific interactions with the nucleobase of G_{-2} while HigA residues Thr34 and Thr37 (both from α3) stably interact with the phosphate of G_{-2}. (**C**) The N- and C-terminal residues of HigA become ordered upon both HigB binding. HigA residue Arg77 forms a hydrogen bond with the backbone carbonyl of Gln3 and Arg2 and Glu80 interact via a salt bridge. (**D**) Comparison of the tetrameric $HigB_2HigA_2$ complex (all black; PDB code 4MCX) and $HigB_2HigA_2$-O2 DNA complex (PDB code 4MCX) reveal a ~14º rotation of $HigB_2HigA_2$ away from DNA that allows recognition.

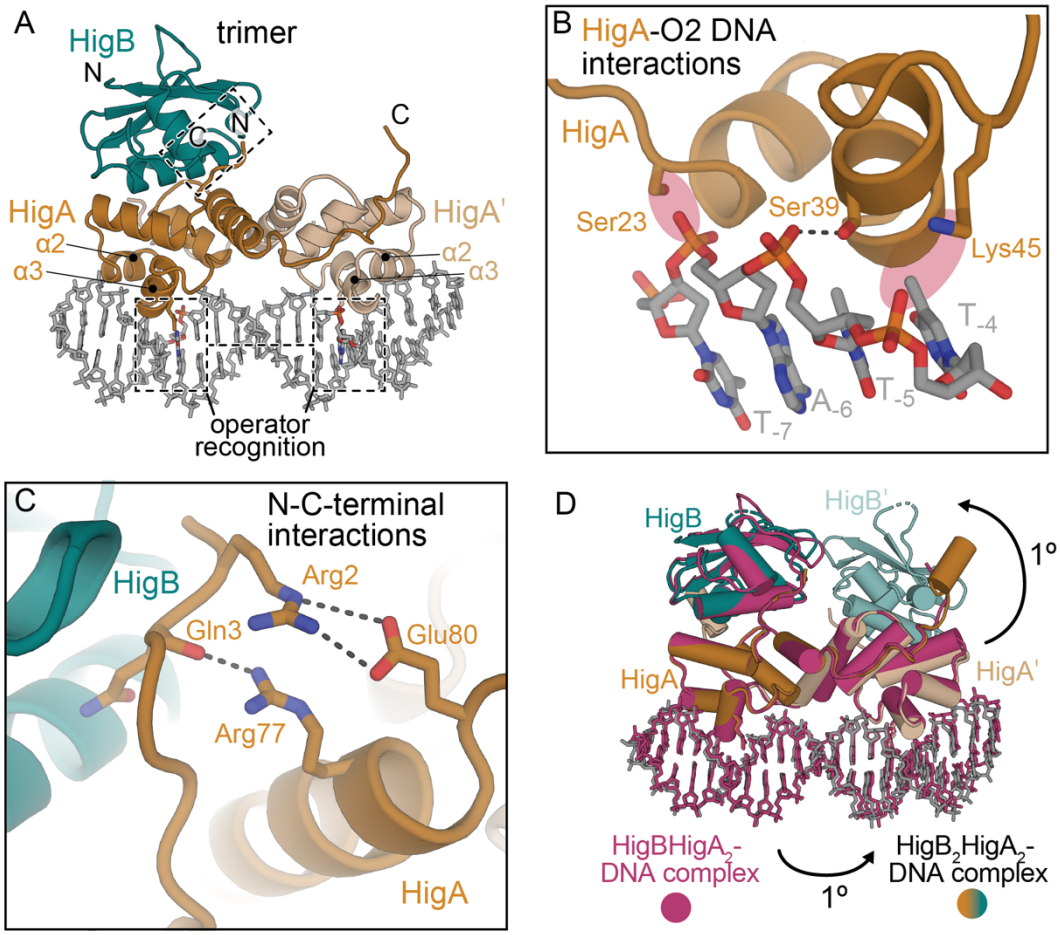

Figure 5. Structure of trimeric HigBHigA$_2$ bound to O2 DNA. The 2.8-Å structure of trimeric HigBHigA$_2$-O2 DNA (PDB code 6WFP). HigA recognizes the T_{+6}, G_{+7}, T_{+8}, A_{+9} DNA region via α2 and α3. N and C-terminal regions of HigA are boxed. (**B**) In the HigB$_2$HigA$_2$-O2 DNA structure (PDB code 6W6U), HigA residues Ser23, Ser39, and Lys45 interact with the backbone phosphate of T_{-7}, T_{-5}, and T_{-4} respectively to rigidify the T_{-1}, G_{-2}, T_{-3}, A_{-4} sequence for nucleotide-specific recognition on the opposite strand. In the trimeric HigBHigA$_2$-O2 structure, only Ser39 interacts with the phosphate backbone and Ser23 and Lys45 are too distant (red highlighted region). (**C**) The N- and C-terminal residues of HigA become ordered upon a single HigB monomer binding similar to when two HigB monomers bind (Fig. 4C). (**D**) Comparison of trimeric HigBHigA$_2$-O2 DNA (pink; PDB code 6WFP) and

857 tetrameric $HigB_2HigA_2$-O2 DNA (PDB code 6W6U) are incredibly similar with an r.m.s.d of
858 0.7 Å (for 1479 equivalent atoms) and less than a ~1º rotation.
859
860
861
862
863
864
865
866
867
868
869
870
871
872
873
874
875
876
877
878
879
880
881

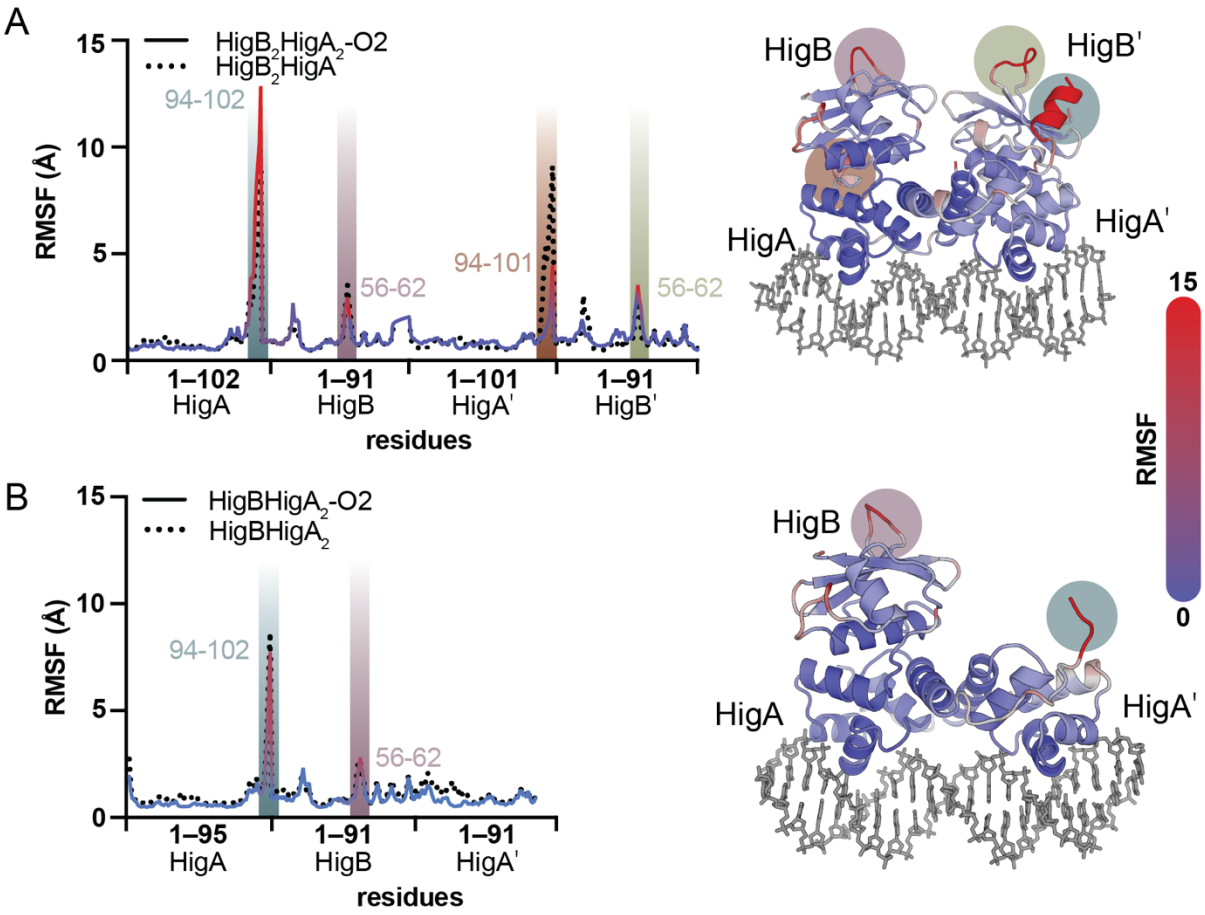

Figure 6. Trimeric HigBHigA$_2$ and tetrameric HigB$_2$HigA$_2$ exhibit similar dynamics in the presence or absence of O2 DNA. Root-mean-square-fluctuations (RMSFs) of Cα atoms for each residue in the (**A**) HigBHigA$_2$ or (**B**) HigB$_2$HigA$_2$ complexes are calculated from 1 ms MD trajectories. Regions that have increased RMSFs are indicated with highlighted bars that correspond to their positions on the HigBHigA-O2 structures (*right*). High RMSF spikes correlate to either labile C-termini of HigA or HigB loop regions with colored circles corresponding to the highlighted bars on the left.

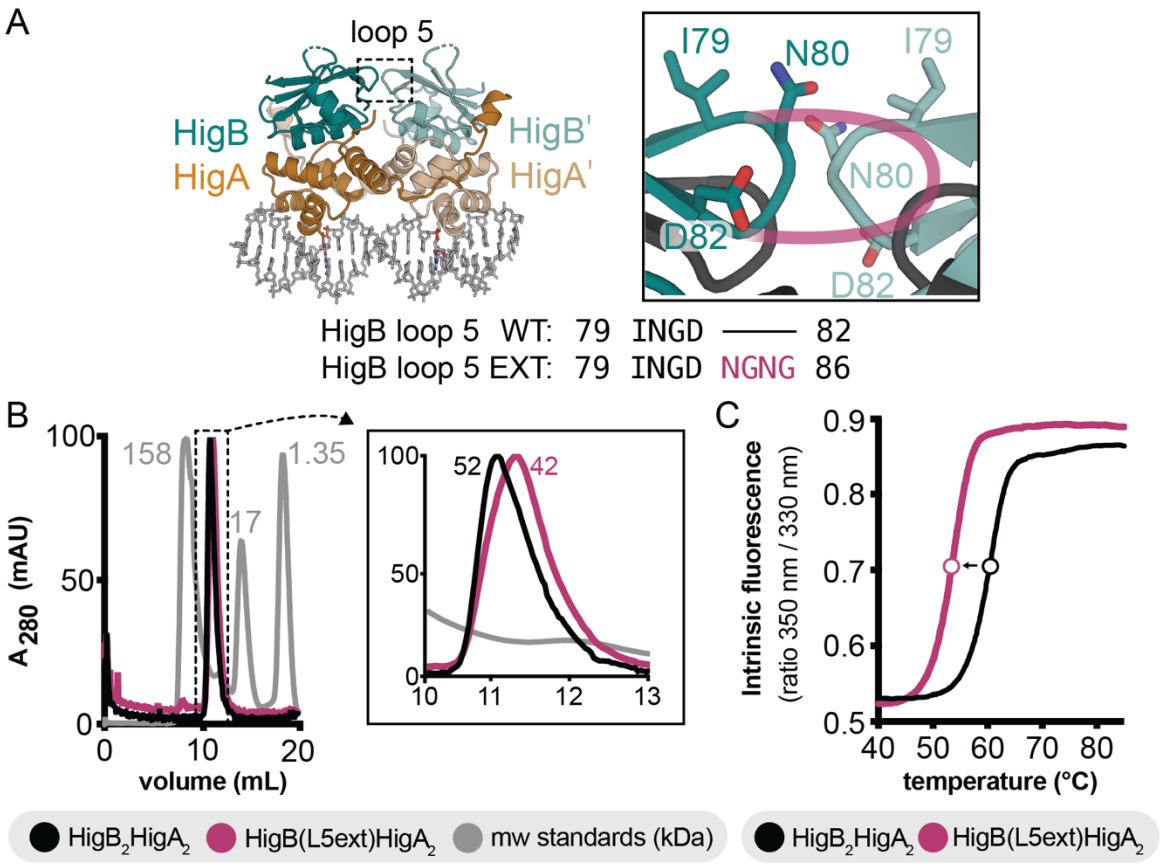

Figure 7. Engineering a trimeric HigBHigA$_2$ complex. (**A**) To prevent two HigB monomers from binding, loop 5 (L5) of HigB was extended by the insertion of four residues (Asn, Gly, Asn, Gly; NGNG; "L5ext", magenta) after residue Asp82. The dotted box indicating the L5 region of two HigB monomers is zoomed in (*right*). The theoretical extension of L5 is shown in magenta with the wild-type HigB and HigB(L5ext) amino acid alignment shown underneath. (**B**) Size exclusion chromatography of purified wild-type HigB$_2$HigA$_2$ shows an elution volume that corresponds to a molecular weight of 52 kDa. HigB(L5ext)HigA$_2$ complex (magenta) elutes at a volume corresponding to a molecular weight of 42 kDa with the inset showing a zoomed in view. Molecular weight standards are shown in grey. (**C**) Nano-DSF analysis of wild-type HigB$_2$HigA$_2$ (black) and HigB(L5ext)HigA$_2$ (magenta) shows that the HigB(L5ext)HigA$_2$ complex has ~5ºC lower T_i value than HigB$_2$HigA$_2$. Fluorescence values

were normalized to the highest tested temperature and the boundary of each line represents the mean ± SD of values of three independent experiments.

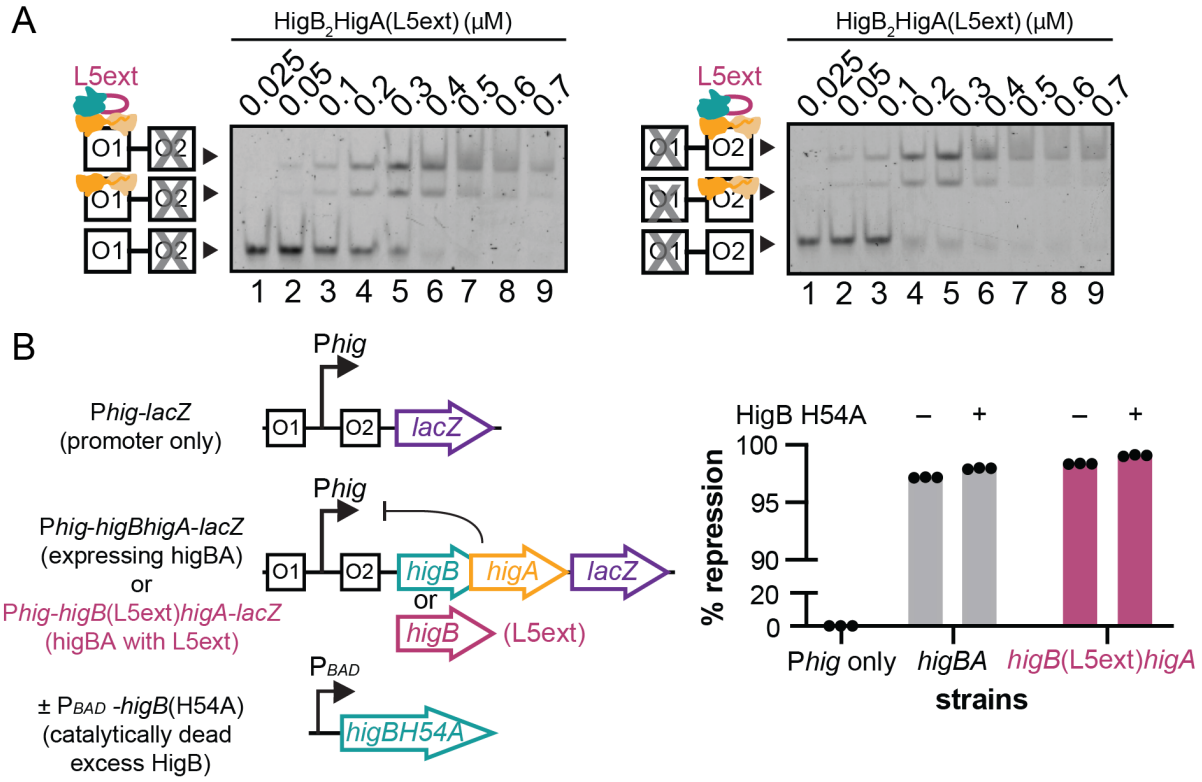

928

929 **Figure 8. Trimeric HigB(L5ext)HigA$_2$ is sufficient to repress transcription of P*hig*.** (**A**)
930 EMSA of HigB(L5ext)HigA$_2$ binding to O1 DNA (O2 scrambled; *left*) or to O2 DNA (O1
931 scrambled; *right*). (**B**) β-gal assays of *E. coli* BW25113 transformed with either pQF50-P*hig-*
932 *lacZ* (P*hig* only), pQF50-P*hig-higBhigA-lacZ* (*higBhigA*), pQF50-P*hig-higB*(L5ext)*higA-lacZ*
933 (*higB*(L5ext)*higA*), and/or pBAD33-*higB*(H54A). P*hig* only demonstrates the maximum
934 amount of β-gal activity (black bar, 0% repression). Constructs containing either a wild-type
935 HigBHigA (grey bars) or a HigB(L5ext)HigA variant (pink bars) both repress transcription
936 (first bar in each group). Excess HigB expression (using a catalytically inactive H54A variant)
937 results in little difference in repression (second bars). Error bars represent the mean ± SD
938 of values of three independent experiments (raw values shown as dots).

939

940